micromachines

MDPI

Article

Liposome Deformation Induced by Membrane-Binding Peptides

Kayano Izumi, Chihiro Saito and Ryuji Kawano *

Department of Biotechnology and Life Science, Tokyo University of Agriculture and Technology, Tokyo 184-8588, Japan
* Correspondence: rjkawano@cc.tuat.ac.jp

Abstract: This paper presents an investigation of liposome deformation and shape distortion using four membrane-binding peptides: TAT and C105Y as cell-penetrating peptides (CPPs), and melittin and ovispirin as antimicrobial peptides (AMPs). Liposome deformation was monitored utilizing fluorescent microscopy, while the binding of peptides to the DOPC membrane was estimated through capacitance measurements. The degree of liposome deformation and shape distortion was found to be higher for the CPPs compared to the AMPs. Additionally, it was observed that C105Y did not induce liposome rupture, unlike the other three peptides. We propose that these variations in liposome distortion may be attributed to differences in secondary structure, specifically the presence of an α-helix or random coil. Our studies offer insight into the use of peptides to elicit control of liposome architecture and may offer a promising approach for regulating the bodies of liposomal molecular robots.

Keywords: liposome deformation; peptide; membrane capacitance

check for updates

Citation: Izumi, K.; Saito, C.; Kawano, R. Liposome Deformation Induced by Membrane-Binding Peptides. *Micromachines* **2023**, *14*, 373. https://doi.org/10.3390/mi14020373

Academic Editors: Ching-Te Kuo and Hsinyu Lee

Received: 26 December 2022
Revised: 25 January 2023
Accepted: 31 January 2023
Published: 2 February 2023

Copyright: © 2023 by the authors. Licensee MDPI, Basel, Switzerland. This article is an open access article distributed under the terms and conditions of the Creative Commons Attribution (CC BY) license (https://creativecommons.org/licenses/by/4.0/).

1. Introduction

Cell-sized liposomes are frequently employed in the study of model cells or cell membranes. They are also utilized in the field of synthetic biology for encapsulating materials, particularly in the realm of "Build-a-Cell" research [1,2]. For instance, various reaction networks utilizing enzymatic and chemical reactions, as well as protein expression, have been implemented within liposomes [3]. Building upon the technologies of synthetic biology, the field of molecular robotics has emerged as a subdiscipline, which shares similarities with "Build-a-Cell" research but addresses challenges from an engineering perspective [4–6]. A molecular "robot" can be defined as a micro-robot consisting of molecules and comprising three essential components: a sensor for perception, a calculator for intelligence, and actuators for motor function. These functionalities are integrated within a micron-sized body surrounded by a lipid membrane. In 2017, Sato et al. reported the prototype of a sophisticated molecular robot, in which they developed an amoeba-type robot with light-induced DNA clutches for sensors and kinesin-microtubule proteins as actuators, all integrated within a cell-sized liposome. Light irradiation serves as a trigger for the release of signaling molecules and engagement of the DNA clutches, leading to a change in the shape of the liposome [7].

The control of liposome shape has been a topic of investigation in molecular robotics, as deformability is a necessary characteristic for movement within micro and crowded environments, such as within living organisms or soil. For example, deformable liposomes containing surfactants have been shown to permeate human skin, enabling the transdermal transport of drugs [8,9]. Several approaches have been proposed to deform liposomes, including the use of surfactants [10,11], proteins [3,12,13], and peptides [14–20]. The use of fatty acid surfactants, such as oleate, has been shown to induce the growth, division, and budding of phospholipid or oleate liposomes [10]. Additionally, surfactants have been demonstrated to induce shape deformation in fatty acid vesicles, with deformation dependent on the type of surfactant; for example, the size of vesicles rapidly increases with

the addition of Triton X-100, and sodium dodecyl sulfate induces changes in membrane curvature [11]. Proteins have also been shown to induce deformation in liposomes through encapsulated polymerization of cytoskeletal components [12]. For example, Furusato et al. expressed several proteins involved in the formation of the Z-ring in bacterial cytokinesis and induced liposome deformation through their presence [3]. Remarkable deformation from spherical to other structures was observed under certain conditions, such as in the presence of FtsZ and ZipA. In the case of using peptides, liposome budding was induced by a partial sequence derived from matrix-2 (M2), a component of the influenza virus [20]. Additionally, various researchers have reported the use of a venom toxin, melittin, to induce liposome deformation. As methodologies for peptide design and synthesis have been significantly advanced in recent decades, peptides have emerged as a potential material for the transformation of molecular robots [21].

We here investigated 1,2-dioleoyl-*sn*-glycero-3-phosphocholine (DOPC) liposome deformation induced by the following four peptides which are known as antimicrobial peptides (AMPs) and cell-penetrating peptides (CPPs) which can spontaneously bind to bilayer lipid membranes:

(1) Human immunodeficiency virus (HIV)-1 tat (TAT, YGRKKRRQRRR, 11 amino acids) is derived from 47–57 amino acids of the HIV-1 transcriptional activator [22–25].

(2) C105Y (CSIPPEVKFNKPFVYLI, 17 amino acids) is a synthetic peptide based on 359–374 residues of α1-antitrypsin [24,26].

(3) Melittin (GIGAVLKVLTTGLPALISWIKRKRQQ, 26 amino acids) is derived from Apis mellifera (a honey bee), and some studies have reported liposome deformation using this peptide [19,27–32].

(4) Ovispirin (KNLRRIIRKIIHIIKKYG, 18 amino acids) is derived from the N-terminal 18 amino acids of SMAP-29 [33,34].

There have been numerous reports on the secondary structures of the peptides at the PC membrane including DOPC. The CPPs, such as TAT and C105Y, have been proposed to exhibit a tendency towards random coil structures [24,25], whereas the AMPs (melittin and ovispirin) have been suggested to primarily adopt an α-helical structure [28,29,33,34]. In this study, we hypothesized that they may also exhibit random coil and amphipathic α-helix structures.

To investigate liposome deformation induced by these peptides, we employed fluorescent microscopy and measured membrane capacitance. The latter approach allows for the determination of changes in membrane properties, such as surface area, permittivity, and thickness, resulting from peptide binding. Based on our results, we evaluated the effectiveness of the peptides in inducing liposome deformation.

2. Materials and Methods

2.1. Experimental Materials

In this study, the following chemicals were used: 1,2-dioleoyl-*sn*-glycero-3-phosphocholine (DOPC; Avanti Polar Lipids, Birmingham, AL, USA), 1,2-dioleoyl-*sn*-glycero-3-phosphoethanolamine-N-(lissamine rhodamine B sulfonyl) (ammonium salt) (Rhodamine PE; Avanti Polar Lipids, Birmingham, AL, USA), liquid paraffin (FUJIFILM Wako Pure Chemical Corporation, Osaka, Japan), calcein (Sigma-Aldrich Co, LCC., St. Louis, MO, USA), glucose (FUJIFILM Wako Pure Chemical Corporation, Osaka, Japan), sucrose (FUJIFILM Wako Pure Chemical Corporation, Osaka, Japan), *n*-decane (FUJIFILM Wako Pure Chemical Corporation, Osaka, Japan), 3-morpholinopropane-1-sulfonic acid (MOPS, Nacalai Tesque, Kyoto, Japan), potassium chloride (KCl, Nacalai Tesque, Kyoto, Japan). As peptides, we used C105Y (GenScuript, Piscataway, NJ, USA), melittin (synthesized and purified as powder), ovispirin (KareBay Biochem, Inc., Monmouth Junction, NJ, USA), and TAT (BACHEM, Bubendorf, Switzerland). Peptides were stored at −20 °C. For use, samples were diluted to their designated concentration using a buffered electrolyte solution and stored at 4 °C.

2.2. Preparation of Giant Liposomes Using the Droplet Transfer Method

Liposomes of 98:2 DOPC/Rhodamine PE (mol %) were prepared using droplet transfer. [35] First, 12.1 μL of 32.6 mM lipid mixture dissolved in chloroform was poured into a glass vial and evaporated under a flow of nitrogen until a lipid film formed at the bottom of the vial. The vial was then put in a desiccator (AZ ONE Corporation, Osaka, Japan) for more than three hours to completely remove the remaining chloroform. Next, 300 μL of liquid paraffin was added to the vial and stirred with the lipids using a 40 kHz ultrasonic cleaner MSC-2 (AZ ONE Corporation, Osaka, Japan) at 50 °C for an hour. Then, a 20 μL liquid mixture of 0.5 M sucrose and 0.5 mM calcein dissolved in MilliQ ultra-pure water (MQ) was added to the vial, and the contents were mixed by tapping 40 times, to form water-oil (W/O) emulsions. 150 μL of the content was slowly added to 150 μL of 0.5 M glucose dissolved in MQ in a 500 μL polycarbonate centrifuge tube and centrifuged at 8000× *g* for 5 min with centrifuge CT15E (Hitachi Koki Co. Ltd., Tokyo, Japan). Giant liposomes were precipitated at the bottom of the tube by the oil-to-water phase transfer of the W/O emulsions. The pellet of the liposomes was extracted, resuspended into a new centrifuge tube with 300 μL of 0.5 M glucose dissolved in MQ, and centrifuged again at 6000× *g* for 10 min to remove small lipid aggregates. After centrifuging twice, the pellets of liposomes were loaded into a new centrifuge tube with 100 μL of 0.5 M glucose dissolved in MQ. All preparations were conducted at room temperature (RT) unless otherwise specified. Liposomes were observed using an IX71 fluorescence microscope (OLYMPUS Corporation, Tokyo, Japan). First, we prepared an observing chamber by punching a 6.0 mm hole in a silicon rubber sheet of 5.0 mm thickness and stuck it on the cover glass. 49 μL of liposomes dissolved in 0.5 M glucose was loaded into the chamber and allowed to settle for at least 15 min to confirm their spherical stability. After the liposomes had settled, 1.0 μL of 50.0 μM peptide dissolved in 0.5 M glucose was gently loaded into the chamber. Thus, the final peptide concentration was 1 μM for each peptide–lipid mixture. To minimize the flow of liposomes, we sunk liposomes near the bottom and observed them in a confined space. The liposomes were observed through a WIG filter (excitation range: 520–550 nm, Hg-lamp). Images were recorded using a DFK33UX252 camera (Argo Corporation, Osaka, Japan). All observations were conducted at RT at least three times. For quantitative analysis, we used Fiji, which is an image-processing package of ImageJ (National Institutes of Health, Bethesda, MD, USA), and Otsu's threshold clustering algorithm [36].

2.3. Image Analysis of Liposomes

In order to evaluate the deformation of liposomes, we conducted a comprehensive analysis comprising three distinct components. The first component, referred to as deformation analysis, involved assessing the frequency with which various peptides were capable of inducing deformation in liposomes. The second component, distortion analysis, focused on quantifying the degree to which each peptide was able to distort liposomes by measuring the average maximum cross-sectional area (ΔA_m) and corresponding time points of five liposomes selected in descending order of aspect ratio (*AR*) after peptide addition. The final component, partial deformation analysis, sought to determine the shape of the local distortion by comparing the partial deformation of individual liposomes before and after peptide addition. To this end, we selected two snapshots within the time-lapse of representative deforming liposomes in each condition: one with the median *AR* before adding peptides to showcase the mean shape of the spherical liposome and another with the ΔA_m after adding any peptide to demonstrate the distortion.

2.4. Measurement of Membrane Capacitance and Subsequent Analysis

Membrane capacitance (C_m) was detected using electrophysiological methodologies. [37] First, we fabricated the body of the detection device to have a 6.0 mm thickness and two separators with 0.2 mm thickness from a polymethyl methacrylate (PMMA) plate using a three-dimensional modeling machine (MM-100, Modia Systems, Saitama, Japan) (Figure S1). Two chambers with a 2.0 mm diameter and a 4.5 mm depth and a groove

with a 0.45 mm width between the wells were carved on the device. A hole with a 1.0 mm diameter was carved in each separator. Each chamber in the device had a hole of 0.5 mm diameter in the bottom, and Ag/AgCl electrodes were set into the hole. A polymeric film made of parylene C (polychloro-p-xylylene) with a 5.0 μm thickness was patterned with a single pore of 100 μm diameter using photolithography. The film was sandwiched by two separators and inserted into the groove of the device to separate the two chambers.

Next, 1.5–2.0 μL of 25.4 μM DOPC dissolved in *n*-decane and 5.0 μL of a liquid mixture of 1 μM peptide, 150 mM KCl, and 10 mM MOPS (pH 7) dissolved in MQ were loaded into chambers in order. To contact the aqueous droplets in two chambers, a bilayer was formed at the parylene pore [38–42]. In addition to applying a +5 mV holding voltage, a +5 mV square pulse was given at a pulse frequency of 40 kHz. When the capacitance reached the upper limit of the measurement equipment, we stop the measurement. To assess the effect of peptide binding on C_m, we measured the temporal parameters such as resistance (R) and time constant (τ) with the capacitance. (See also the result) [43]. All data were recorded with an Axopatch 200B amplifier (Molecular Devices, San Jose, CA, USA) and trials more than n $\geq$ 3. The recorded data were analyzed with the Clampex 9.0 software (Molecular Devices, San Jose, CA, USA).

3. Results

3.1. Microscopic Observation of the Deformation and Rupture of Liposomes by Peptides

Deformation of liposomes was observed through the utilization of fluorescent microscopy for a duration of 30 min following the addition of a peptide at a concentration of 1 μM. To ensure an adequate resolution, only spherical liposomes with a diameter of approximately 6.0 μm were selected; the size distribution is depicted in Figure S2. Upon monitoring the liposomes, it was observed that some liposomes temporarily disappeared due to rupture (as illustrated in Figure S3). When adding TAT, melittin, or ovisprin, more than 80% of liposomes were ruptured within 30 min. In the case of control (without peptide) and C105Y addition, the liposomes were stable, and the rupture was not observed for 30 min (Figure 1a). Liposome deformation was observed in all cases after adding the peptide, and the contour of liposomes fluctuated erratically (distortion), or the size of the liposomes had changed when compared with the control experiment (Figure 1b–f). Liposome deformation was analyzed from two parameters: the temporal change of aspect ratio (AR) and the change of cross-sectional area (ΔA) as defined below:

$$AR = \frac{L_l}{L_s} \tag{1}$$

$$\Delta A = \frac{A_t}{A_{ave.}} \tag{2}$$

where L_s and L_l are the shortest and longest diameter of a given liposome, A_t is the apparent cross-sectional area at t seconds after adding the peptides and $A_{ave.}$ is an average cross-sectional area for a minute before adding peptides, respectively.

Liposomes seem to be slightly deforming without peptides probably due to the convection of the solution. We defined a threshold of large deformation by AR and ΔA based on the data of the absence of peptides. Deformation of liposomes in this study was defined as over the threshold:

$AR > 1.1$

$\Delta A > 1.1$

The AR and the ΔA provide information on the shape distortion and the size change of liposomes. The order of AR at 30 min was as follows (Figure 1c–f):

TAT > C105Y = ovispirin = melittin

The order of ΔA was:

TAT > C105Y > ovispirin = melittin

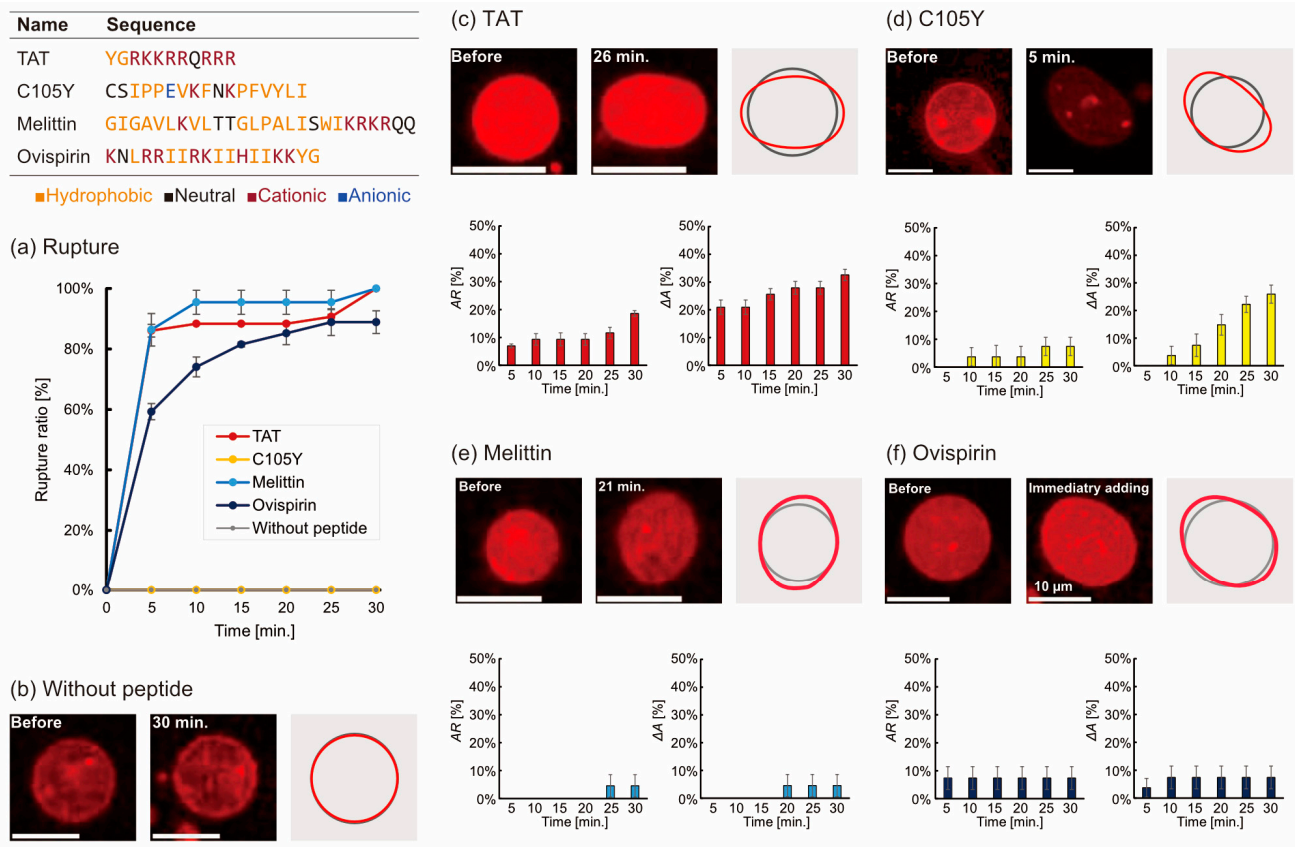

Figure 1. (**a**) The rupture ratio of liposomes during 30 min after adding five peptides. (**b**) Images of liposomes without peptide and (**c**–**f**) with 1 μM peptide addition. The grey line and red line in the right of the images are the tracing outlines of the liposomes before and after adding peptides. The bar graphs show the time dependence of the deforming ratio of *AR* and Δ*A*. The number of trials N ≥ 3 and the number of liposomes n = 10 without peptide and n > 20 with peptide.

We next analyzed these deformation parameters in detail: the distortion estimated by the *AR*, and the size change estimated by the Δ*A* (Figure 2a,b). Regarding the *AR*, the maximum *AR* (AR_m) ranged from 1.1 to 1.4, and TAT showed the highest AR_m (Figure 2c). The order of AR_m was:

TAT > C105Y > ovispirin = melittin

The observed AR_m occurred at different times during the 30 min for each peptide. Melittin and ovispirin reached the AR_m within 10 min, whereas that of TAT and C105Y were over 10 min (Figure 2d). The time order was similar to the result of *AR* as follows:

TAT > C105Y > melittin > ovispirin

As for the Δ*A*, the maximum Δ*A* (ΔA_m) ranged from 1.1 to 1.4, and TAT also showed the highest ΔA_m (Figure 2e). The order was similar to the result of *AR* as follows:

TAT > C105Y > melittin = ovispirin

These ΔA_m were observed before 10 min except for C105Y (Figure 2f). The time order was as follows:

C105Y > melittin ≥ ovispirin > TAT

The quantitative estimation of the distortion was performed by analyzing the angle-dependence radius of liposomes as previously proposed in the literature [3]. The normalized radius ($R_{nor.}$) was calculated based on an equation:

$$R_{nor.} = \frac{R(\theta)}{R_{ave.}} \quad (3)$$

where $R_{ave.}$ is the average radius, and $R(\theta)$ is the radius at each angle (θ), respectively. The radius of each peptide against the angles is depicted in Figure 2g. The TAT (0.18 ± 0.01)

and C105Y (0.15 ± 0.03) system tended to show a higher amplitude of $R_{nor.}$ than that of the melittin (0.10 ± 0.02) and ovispirin (0.12 ± 0.01) system.

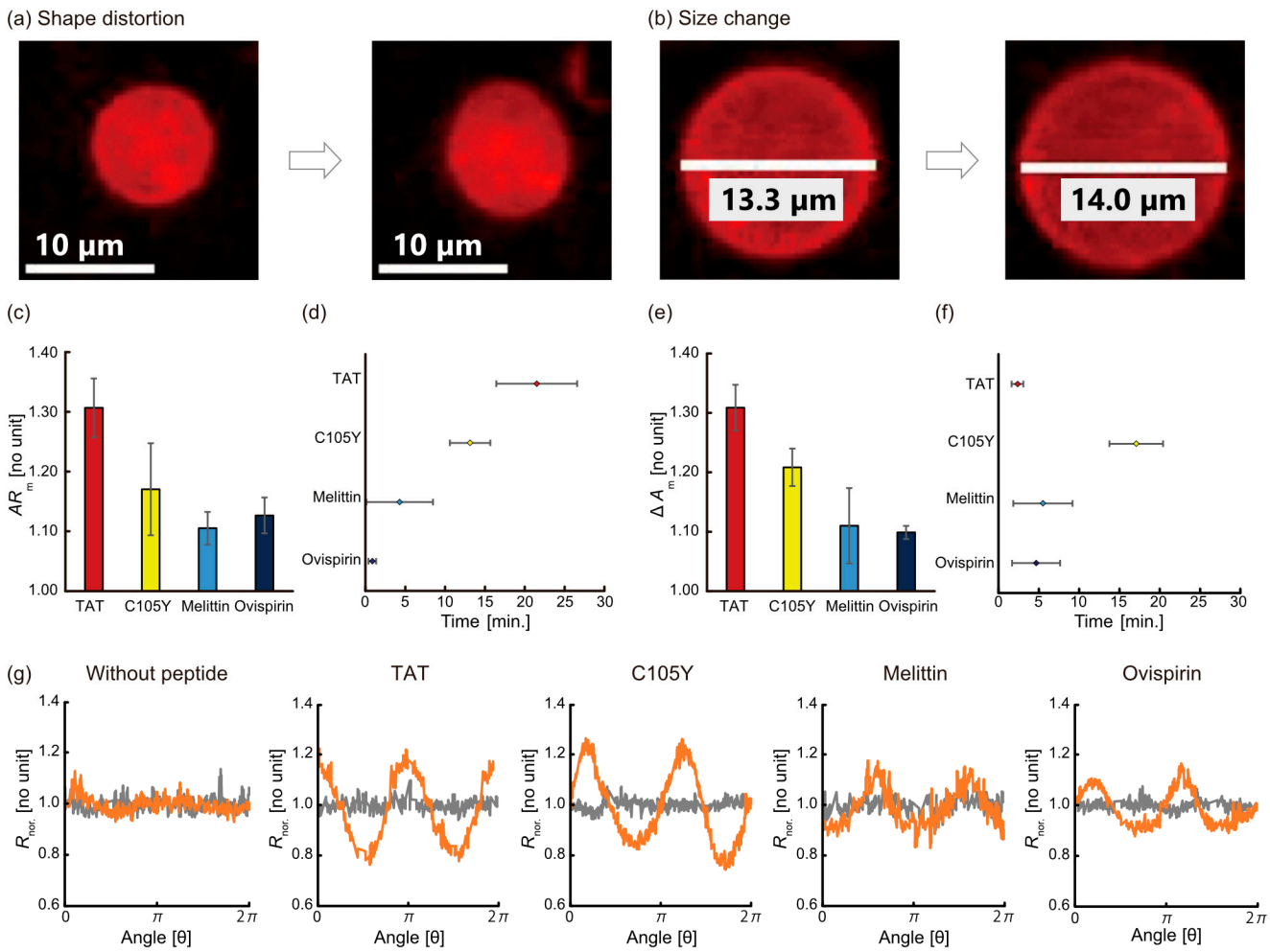

Figure 2. Typical images of the liposome deformation of (**a**) shape distortion and (**b**) size change before and after adding peptides. (**c**) The maximum AR (AR_{m}) in the case of adding each peptide. (**d**) The time of the maximum AR (AR_{m}). (**e**) The maximum ΔA (ΔA_{m}) in the case of adding each peptide. (**f**) The time of maximum ΔA (ΔA_{m}). (**g**) Partial distortion for each condition. The distortions at each angle before (gray) and after adding peptides (orange) were quantified by the deviation of the relative distance from 1.0 indicating the radius of true circle.

3.2. Binding of Peptide on the Lipid Membrane Estimated by the Membrane Capacitance

It has previously been reported that the capacitance of lipid membranes (C_m) increases with the binding of added antimicrobial peptides [44]. In this study, we estimated the binding of peptides TAT, C105Y, melittin, and ovispirin to the lipid membrane by measuring the increase in C_m. These peptides have the ability to form pores or defects during capacitance measurement; thus, we considered the effect of leakage current on C_m. A general capacitance (C) is given by the following equation:

$$C = QV \tag{4}$$

where Q is the charge amount and V is the applied voltage.

Leakage current should affect the value of current and resistance if the leaking has occurred. In our experimental system, the temporal current in the circuit ($I(t)$) is calculated in the following equation [36]:

$$I_{(t)} = \frac{V}{R_m + R_s}\left(1 + \frac{R_m}{R_s}e^{-\frac{t}{\tau}}\right) \tag{5}$$

$$\text{where } \tau = \frac{R_m\, R_s\, C_m}{R_m + R_s} \tag{6}$$

In the equations, R_m is membrane resistance, R_s is the series resistance, total resistance except for R_m, V is the square pulse voltage, and τ is the time constant. R_s and V are constant, and R_m and C_m can be affected by the change in current. Equation (6) can be approximated as follow because the $R_m >> R_s$ in our measurements:

$$\tau \fallingdotseq \frac{R_m \cdot R_s \cdot C_m}{R_m} = R_s \cdot C_m \tag{7}$$

Since R_s is constant, the C_m is proportional to τ:

$$\tau \propto C_m \tag{8}$$

In order to eliminate the influence of leakage currents on our measurements, we established time zero as the point at which the capacitance (C_m) begins to be proportional to the time constant of current decay (Figure S4). For the purposes of analysis, we restricted our data to that which adhered to Equations (5)–(8), as the purpose was to estimate the change in C_{m} resulting from peptide binding, rather than the effect of leakage currents. Our calculations indicate that the impact of leakage currents on the continuous increase in C_m was minimal. In the absence of the peptides, C_m initially increased and then reached a plateau state, as depicted in Figure 3a. This transition from the initial state to the plateau state is indicative of a shift from lipid monolayer to thinner bilayer formation, as observed through the droplet contact method employed in this study [45]. In contrast, in the presence of the peptide, the C_m in the majority of measurements gradually increased from the initial state and did not reach a plateau state, instead reaching the upper limit of the equipment within a matter of minutes (Figure 3b–e). The normalized C_m ($C_{nor.}$) was calculated in the following equation:

$$C_{nor.} = \frac{C_{max}}{C_i} \tag{9}$$

where C_{max} is the maximum C_m and C_i is the initial C_m at the starting time of the measurements (=time 0). The $C_{nor.}$ ranged from 1.3 to 1.5 without peptides and from 1.6 to 4.2 with peptides.

We next estimated that the continuous increase showed the peptide binding. Based on Equation (9), we considered what parameter(s) reflect the increase of the C_m.

The C_m can be defined as:

$$C_m = \varepsilon_0 \varepsilon_r \frac{S}{d} \tag{10}$$

where parameters ε_0, ε_r, S, and d are the permittivity of a vacuum, relative permittivity, surface area, and thickness of the planar bilayer lipid membrane, respectively. The capacitance data allows us to infer that peptides are binding to the membrane, as the parameters can vary in response to peptide binding. The variations in the effective lipid bilayer area (S) and the thickness of the membrane are expected to be minimal in comparison to the changes in ε_r as the ε_r value of peptides (around 54) [46] is significantly greater than that of DOPC molecules (around 2 to 3) (Figure S5) [47]. Therefore, we consider that the increase in C_m is due to peptides binding to the lipid membrane and an increase in peptide binding resulting in the ε_r increase. In addition, the ε_r change of the four peptides was similar (around 40 pF,

n ≥ 3, the control was ca. 10 pF, n = 3), indicating a comparable amount of bindings to the lipid membrane.

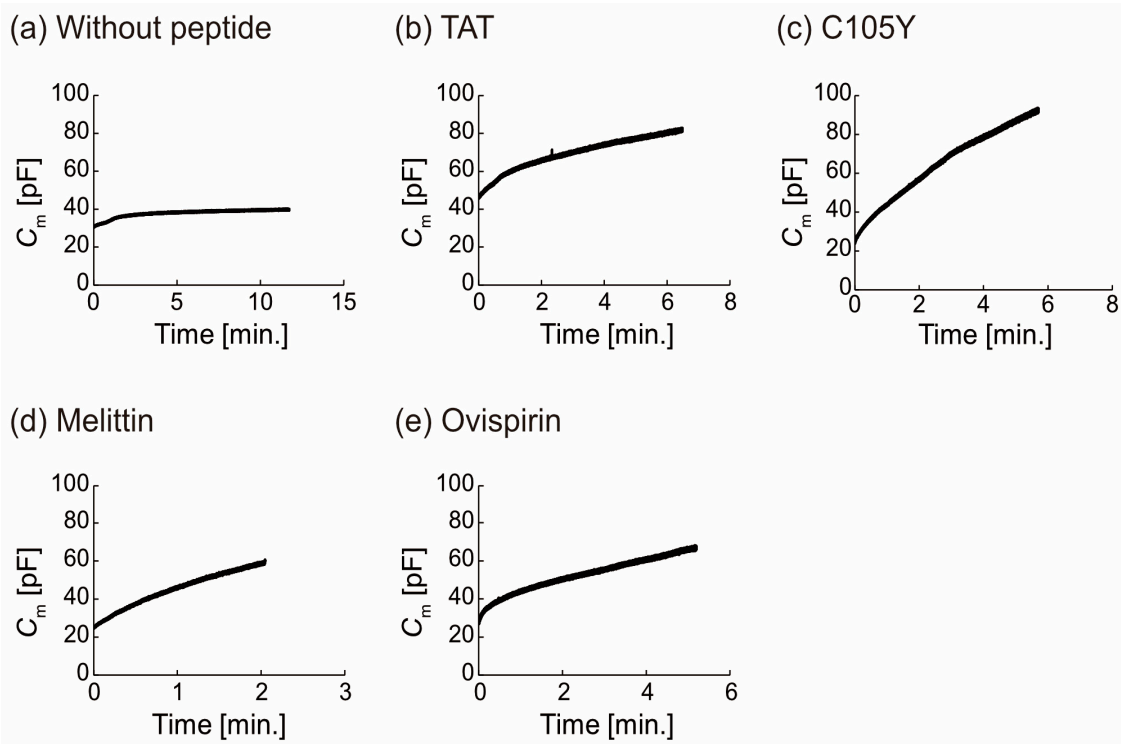

Figure 3. Membrane capacitance measurements for estimating the peptide binding in the lipid membrane. (**a**) without peptide, (**b**–**e**) with peptide.

4. Discussion

The ability of four peptides, TAT (CPP), C105Y (CPP), melittin (AMP), and ovispirin (AMP), to induce liposome deformation was investigated utilizing fluorescence microscopy and membrane capacitance measurements. The findings of this study revealed that C105Y did not exhibit the ability to rupture liposomes, unlike the other three peptides, which caused the disappearance of over 70% of liposomes within 10 min. The amphipathicity of peptides was found to be a significant factor in the ability to rupture liposomes. [48] C105Y (17 aa.) has a Glu and two Lys at the 6th, 8th, and 11th positions, and its charge distribution sequence imparts a relatively low degree of amphipathicity [24,26]. In contrast, the other three peptides possess relatively stronger amphipathicity due to their amphipathic α-helical structure (melittin and ovispirin) and charge polarization structure (TAT).

We next found that the capability of liposome deformation used in TAT and C105Y was greater than that in melittin and ovispirin. Initially, it was hypothesized that this difference was due to variations in the amount of peptide binding to the lipid membrane. However, subsequent membrane capacitance measurements revealed that the binding of peptides was almost equivalent among the peptides. Therefore, the observed difference in deformation may be attributed to variations in the secondary structure of the peptides, which leads to distinct interactions and localization within the lipid membrane. Peptides with random coil structures display random-like behavior within the lipid membrane, [24,25], and it has been proposed that conventional CPPs bind to lipid membranes and exhibit behavior akin to that of detergents or form inverted micelle structures. [24,25]. In contrast, peptides with an α-helical structure have amphiphilic properties upon binding to the surface of the lipid membrane and tend to form a transmembrane structure or cover the surface in a carpet-like manner [19,28–34]. This hypothesis is supported by molecular dynamics simulation (see also supporting description and Figure S6) [49–54]. The secondary structure and

the membrane-binding mode of these peptides have a significant impact on macroscopic membrane deformation in liposomes.

5. Conclusions

In conclusion, we investigated the ability of four distinct peptides, CPPs and AMPs, to induce liposome deformation. The deformation and rupture of liposomes were monitored using fluorescent microscopy. It was observed that C105Y did not induce liposome rupture and that the degree of deformation and shape distortion varied between TAT and C105Y (CPPs) and melittin and ovispirin (AMPs). The binding of peptides to the lipid membrane was estimated using membrane capacitance (C_m) measurements, which indicated that there was not a significant difference in the amount of peptide binding among the peptides. These variations in the effects on liposome deformation may be attributed to variations in the secondary structures of the peptides when bound to a DOPC membrane. Our studies provide insight into the utilization of peptides to control liposome shape and offer a promising approach for regulating the bodies of liposomal molecular robots. In future research, we will design peptides capable of controlling liposome deformation, incorporate these peptides into liposomes, and modulate liposome deformation depending on the context.

Supplementary Materials: The following supporting information can be downloaded at: https://www.mdpi.com/article/10.3390/mi14020373/s1, Figure S1: the device of capacitance measurement; Figure S2: size distribution of analyzed liposomes; Figure S3: rupture of liposomes; Figure S4: the principle of capacitance detection; Figure S5: correlation between physical parameters and physical parameters at the membrane; Figure S6: all-atom MD simulation for the migration of 400 ns

Author Contributions: R.K. conceived the original idea; K.I. conducted all experiments and analyzed the data in this article; C.S. conducted the MD simulation; K.I. and R.K. wrote the paper. All authors have read and agreed to the published version of the manuscript.

Funding: This research was partially supported by JSPS KAKENHI, grant numbers 21K19786 (R.K.), and 21H05229 (R.K.). This work was also supported by the Support for Pioneering Research Initiated by the Next Generation of FLOuRISH Institute, Tokyo University of Agriculture and Technology (TUAT) granted by the Ministry of Education, Culture, Sports, Science and Technology (MEXT), Japan (K.I.), and by the proposal-based Project Fund by the WISE program (K.I.).

Institutional Review Board Statement: Not applicable.

Informed Consent Statement: Not applicable.

Data Availability Statement: Not applicable.

Acknowledgments: The authors thank N. Saigo, K. Shimizu, S. Fujita and Z. Peng in our group, and T. Inoue, and H. Matsubayashi of Johns Hopkins University for constructive discussion and advice on data analysis.

Conflicts of Interest: The authors declare no conflict of interest.

References

1. Sun, J.; Rijpkema, S.J.; Luan, J.; Zhang, S.; Wilson, D.A. Generating biomembrane-like local curvature in polymersomes via dynamic polymer insertion. *Nat. Commun.* **2021**, *12*, 2235. [CrossRef] [PubMed]
2. Chen, Z.; Wang, J.; Sun, W.; Archibong, E.; Kahkoska, A.R.; Zhang, X.; Lu, Y.; Ligler, F.S.; Buse, J.B.; Gu, Z. Synthetic beta cells for fusion-mediated dynamic insulin secretion. *Nat. Chem. Biol.* **2018**, *14*, 86–93. [CrossRef]
3. Furusato, T.; Horie, F.; Matsubayashi, H.T.; Amikura, K.; Kuruma, Y.; Ueda, T. De Novo Synthesis of Basal Bacterial Cell Division Proteins FtsZ, FtsA, and ZipA Inside Giant Vesicles. *ACS Synth. Biol.* **2018**, *7*, 953–961. [CrossRef]
4. Hagiya, M.; Konagaya, A.; Kobayashi, S.; Saito, H.; Murata, S. Molecular Robots with Sensors and Intelligence. *Acc. Chem. Res.* **2014**, *47*, 1681–1690. [CrossRef] [PubMed]
5. Kawano, R. Synthetic Ion Channels and DNA Logic Gates as Components of Molecular Robots. *Chemphyschem* **2018**, *19*, 359–366. [CrossRef] [PubMed]
6. Shoji, K.; Kawano, R. Recent Advances in Liposome-Based Molecular Robots. *Micromachines* **2020**, *11*, 788. [CrossRef]

7. Sato, Y.; Hiratsuka, Y.; Kawamata, I.; Murata, S.; Nomura, S.-I.M. Micrometer-sized molecular robot changes its shape in response to signal molecules. *Sci. Robot.* **2017**, *2*, eaal3735. [CrossRef]
8. Ha, J.H.; Jeong, Y.J.; Kim, A.Y.; Hong, I.K.; Lee, N.H.; Park, S.N. Preparation and Physicochemical Properties of a Cysteine Derivative-Loaded Deformable Liposomes in Hydrogel for Enhancing Whitening Effects. *Eur. J. Lipid Sci. Technol.* **2018**, *120*, 1800125. [CrossRef]
9. Kim, A.R.; An, H.J.; Jang, E.S.; Lee, J.D.; Park, S.N. Preparation, Physical Characterization, and In Vitro Skin Permeation of Deformable Liposomes Loaded with Taxifolin and Taxifolin Tetraoctanoate. *Eur. J. Lipid Sci. Technol.* **2019**, *121*, 1800501. [CrossRef]
10. Peterlin, P.; Arrigler, V.; Kogej, K.; Svetina, S.; Walde, P. Growth and shape transformations of giant phospholipid vesicles upon interaction with an aqueous oleic acid suspension. *Chem. Phys. Lipids* **2009**, *159*, 67–76. [CrossRef]
11. Sudbrack, T.P.; Archilha, N.L.; Itri, R.; Riske, K.A. Observing the Solubilization of Lipid Bilayers by Detergents with Optical Microscopy of GUVs. *J. Phys. Chem. B* **2011**, *115*, 269–277. [CrossRef] [PubMed]
12. Cortese, D.; Schwab, B., III; Frieden, C.; Elson, E.L. Actin polymerization induces a shape change in actin-containing vesicles. *Proc. Natl. Acad. Sci. USA* **1989**, *86*, 5773–5777. [CrossRef] [PubMed]
13. Tanaka, S.; Takiguchi, K.; Hayashi, M. Repetitive stretching of giant liposomes utilizing the nematic alignment of confined actin. *Commun. Phys.* **2018**, *1*, 18. [CrossRef]
14. Lee, M.-T.; Hung, W.-C.; Chen, F.-Y.; Huang, H.W. Mechanism and kinetics of pore formation in membranes by water-soluble amphipathic peptides. *Proc. Natl. Acad. Sci. USA* **2008**, *105*, 5087–5092. [CrossRef]
15. Lee, M.-T.; Sun, T.-L.; Hung, W.-C.; Huang, H.W. Process of inducing pores in membranes by melittin. *Proc. Natl. Acad. Sci. USA* **2013**, *110*, 14243–14248. [CrossRef] [PubMed]
16. Yu, Y.; Vroman, J.A.; Bae, S.C.; Granick, S. Vesicle Budding Induced by a Pore-Forming Peptide. *J. AM. CHEM. SOC.* **2010**, *132*, 195–201. [CrossRef] [PubMed]
17. Takahashi, T.; Nomura, F.; Yokoyama, Y.; Tanaka-Takiguchi, Y.; Homma, M.; Takiguchi, K. Multiple membrane interactions and versatile vesicle deformations elicited by melittin. *Toxins* **2013**, *5*, 637–664. [CrossRef]
18. Yu, Q.; Sun, J.; Huang, S.; Chang, H.; Bai, Q.; Chen, Y.-X.; Liang, D. Inward Budding and Endocytosis of Membranes Regulated by de Novo Designed Peptides. *Langmuir* **2018**, *34*, 6183–6193. [CrossRef]
19. Mally, M.; Majhenc, J.; Svetina, S.; Zeks, B. The response of giant phospholipid vesicles to pore-forming peptide melittin. *Biochim. Biophys. Acta* **2007**, *1768*, 1179–1189. [CrossRef]
20. Rossman, J.S.; Jing, X.; Leser, G.P.; Lamb, R.A. Influenza virus M2 protein mediates ESCRT-independent membrane scission. *Cell* **2010**, *142*, 902–913. [CrossRef]
21. Shimizu, Y.; Inoue, A.; Tomari, Y.; Suzuki, T.; Yokogawa, T.; Nishikawa, K.; Ueda, T. Cell-free translation reconstituted with purified components. *Nat. Biotechnol.* **2001**, *19*, 751–755. [CrossRef] [PubMed]
22. Stalmans, S.; Bracke, N.; Wynendaele, E.; Gevaert, B.; Peremans, K.; Burvenich, C.; Polis, I.; Spiegeleer, B.D. Cell-Penetrating Peptides Selectively Cross the Blood-Brain Barrier In Vivo. *PLoS ONE* **2015**, *10*, e0139652. [CrossRef] [PubMed]
23. Li, S.; Zhang, X.; Guo, C.; Peng, Y.; Liu, X.; Wang, B.; Zhuang, R.; Chang, M.; Wang, R. Hydrocarbon staple constructing highly efficient alpha-helix cell-penetrating peptides for intracellular cargo delivery. *Chem. Commun.* **2020**, *56*, 15655–15658. [CrossRef] [PubMed]
24. Kumara, B.T.; Wijesiri, N.K.; Rathnayake, P.V.G.M.; Ranatunga, R.J.K.U. A Re-evaluation of the Free Energy Profiles for Cell-Penetrating Peptides Across DOPC Membranes. *Int. J. Pept. Res. Ther.* **2021**, *27*, 2931–2943. [CrossRef]
25. Herce, H.D.; Garcia, A.E. Molecular dynamics simulations suggest a mechanism for translocation of the HIV-1 TAT peptide across lipid membranes. *Proc. Natl. Acad. Sci. USA* **2007**, *104*, 20805–20810. [CrossRef]
26. Rhee, M.; Davis, P. Mechanism of uptake of C105Y, a novel cell-penetrating peptide. *J. Biol. Chem.* **2006**, *281*, 1233–1240. [CrossRef]
27. Guha, S.; Ghimire, J.; Wu, E.; Wimley, W.C. Mechanistic Landscape of Membrane-Permeabilizing Peptides. *Chem. Rev.* **2019**, *119*, 6040–6085. [CrossRef]
28. Irudayam, S.J.; Pobandt, T.; Berkowitz, M.L. Free energy barrier for melittin reorientation from a membrane-bound state to a transmembrane state. *J. Phys. Chem. B* **2013**, *117*, 13457–13463. [CrossRef]
29. Krauson, A.J.; He, J.; Wimley, W.C. Gain-of-function analogues of the pore-forming peptide melittin selected by orthogonal high-throughput screening. *J. Am. Chem. Soc.* **2012**, *134*, 12732–12741. [CrossRef]
30. Nguyen, L.T.; Haney, E.F.; Vogel, H.J. The expanding scope of antimicrobial peptide structures and their modes of action. *Trends Biotechnol.* **2011**, *29*, 464–472. [CrossRef]
31. Miyazaki, Y.; Okazaki, S.; Shinoda, W. Free energy analysis of membrane pore formation process in the presence of multiple melittin peptides. *Biochim. Biophys. Acta Biomembr.* **2019**, *1861*, 1409–1419. [CrossRef] [PubMed]
32. Geitani, R.; Moubareck, C.A.; Xu, Z.; Karam Sarkis, D.; Touqui, L. Expression and Roles of Antimicrobial Peptides in Innate Defense of Airway Mucosa: Potential Implication in Cystic Fibrosis. *Front. Immunol.* **2020**, *11*, 1198. [CrossRef] [PubMed]
33. Yamaguchi, S.; Huster, D.; Waring, A.; Lehrer, R.I.; Kearney, W.; Tack, B.F.; Hong, M. Orientation and Dynamics of an Antimicrobial Peptide in the Lipid Bilayer by Solid-State NMR Spectroscopy. *Biophys. J.* **2001**, *81*, 2203–2214. [CrossRef] [PubMed]
34. Woys, A.M.; Lin, Y.-S.; Reddy, A.S.; Xiong, W.; Pablo, J.J.d.; Skinner, J.L.; Zanni, M.T. 2D IR Line Shapes Probe Ovispirin Peptide Conformation and Depth in Lipid Bilayers. *J. Am. Chem. Soc.* **2010**, *132*, 2832–2838. [CrossRef] [PubMed]
35. Pautot, S.; Frisken, B.J.; Weitz, D.A. Engineering asymmetric vesicles. *Proc. Natl. Acad. Sci. USA* **2003**, *100*, 10718–10721. [CrossRef]

36. Schindelin, J.; Arganda-Carreras, I.; Frise, E.; Kaynig, V.; Longair, M.; Pietzsch, T.; Preibisch, S.; Rueden, C.; Saalfeld, S.; Schmid, B.; et al. Fiji: An open-source platform for biological-image analysis. *Nat. Methods* **2012**, *9*, 676–682. [CrossRef]
37. Kawano, R.; Tsuji, Y.; Sato, K.; Osaki, T.; Kamiya, K.; Hirano, M.; Ide, T.; Miki, N.; Takeuchi, S. Automated Parallel Recordings of Topologically Identified Single Ion Channels. *Sci. Rep.* **2013**, *3*, 1995. [CrossRef]
38. Sekiya, Y.; Sakashita, S.; Shimizu, K.; Usui, K.; Kawano, R. Channel current analysis estimates the pore-formation and the penetration of transmembrane peptides. *Analyst* **2018**, *143*, 3540–3543. [CrossRef]
39. Sekiya, Y.; Shimizu, K.; Kitahashi, Y.; Ohyama, A.; Kawamura, I.; Kawano, R. Electrophysiological Analysis of Membrane Disruption by Bombinin and Its Isomer Using the Lipid Bilayer System. *ACS Appl. Bio. Mater.* **2019**, *2*, 1542–1548. [CrossRef]
40. Shimizu, K.; Mijiddorj, B.; Usami, M.; Mizoguchi, I.; Yoshida, S.; Akayama, S.; Hamada, Y.; Ohyama, A.; Usui, K.; Kawamura, I.; et al. De novo design of a nanopore for single-molecule detection that incorporates a beta-hairpin peptide. *Nat. Nanotechnol.* **2022**, *17*, 67–75. [CrossRef]
41. Watanabe, H.; Gubbiotti, A.; Chinappi, M.; Takai, N.; Tanaka, K.; Tsumoto, K.; Kawano, R. Analysis of Pore Formation and Protein Translocation Using Large Biological Nanopores. *Anal. Chem.* **2017**, *89*, 11269–11277. [CrossRef] [PubMed]
42. Hirano, M.; Saito, C.; Yokoo, H.; Goto, C.; Kawano, R.; Misawa, T.; Demizu, Y. Development of Antimicrobial Stapled Peptides Based on Magainin 2 Sequence. *Molecules* **2021**, *26*, 444. [CrossRef] [PubMed]
43. Okada, Y. *Saishin Pacchikuranpu Zikkengizyutsuhou (How to Use Patch-Clamp Method)*; Yoshioka Shoten: Kyoto, Japan, 2011.
44. Hagge, S.O.; Wiese, A.; Seydel, U.; Gutsmann, T. Inner Field Compensation as a Tool for the Characterization of Asymmetric Membranes and Peptide-Membrane Interactions. *Biophys. J.* **2004**, *86*, 913–922. [CrossRef] [PubMed]
45. Funakoshi, K.; Suzuki, H.; Takeuchi, S. Lipid Bilayer Formation by Contacting Monolayers in a Microfluidic Device for Membrane Protein Analysis. *Anal. Chem.* **2006**, *78*, 8169–8174. [CrossRef] [PubMed]
46. Glattli, A.; Chandrasekhar, I.; van Gunsteren, W.F. A molecular dynamics study of the bee venom melittin in aqueous solution, in methanol, and inserted in a phospholipid bilayer. *Eur. Biophys. J.* **2006**, *35*, 255–267. [CrossRef]
47. Valincius, G.; Heinrich, F.; Budvytyte, R.; Vanderah, D.J.; McGillivray, D.J.; Sokolov, Y.; Hall, J.E.; Losche, M. Soluble amyloid beta-oligomers affect dielectric membrane properties by bilayer insertion and domain formation: Implications for cell toxicity. *Biophys. J.* **2008**, *95*, 4845–4861. [CrossRef] [PubMed]
48. Sun, D.; Forsman, J.; Woodward, C.E. Amphipathic membrane-active peptides recognize and stabilize ruptured membrane pores: Exploring cause and effect with coarse-grained simulations. *Langmuir* **2015**, *31*, 752–761. [CrossRef]
49. Van Der Spoel, D.; Lindahl, E.; Hess, B.; Groenhof, G.; Mark, A.E.; Berendsen, H.J. GROMACS: Fast, flexible, and free. *J. Comput. Chem.* **2005**, *26*, 1701–1718. [CrossRef]
50. Huang, J.; Rauscher, S.; Nawrocki, G.; Ran, T.; Feig, M.; de Groot, B.L.; Grubmüller, H.; MacKerell, A.D., Jr. CHARMM36m: An improved force field for folded and intrinsically disordered proteins. *Nat. Methods* **2017**, *14*, 71–73. [CrossRef]
51. Jo, S.; Kim, T.; Iyer, V.G.; Im, W. CHARMM-GUI: A web-based graphical user interface for CHARMM. *J. Comput. Chem.* **2008**, *29*, 1859–1865. [CrossRef]
52. Parrinello, M.; Rahman, A. Polymorphic transitions in single crystals: A new molecular dynamics method. *J. Appl. Phys.* **1981**, *52*, 7182–7190. [CrossRef]
53. Essmann, U.; Perera, L.; Berkowitz, M.L.; Darden, T.; Lee, H.; Pedersen, L.G. A smooth particle mesh Ewald method. *J. Chem. Phys.* **1995**, *103*, 8577–8593. [CrossRef]
54. Hess, B.; Bekker, H.; Berendsen, H.J.C.; Fraaije, J.G.E.M. LINCS: A linear constraint solver for molecular simulations. *J. Comput. Chem.* **1998**, *18*, 1463–1472. [CrossRef]

Disclaimer/Publisher's Note: The statements, opinions and data contained in all publications are solely those of the individual author(s) and contributor(s) and not of MDPI and/or the editor(s). MDPI and/or the editor(s) disclaim responsibility for any injury to people or property resulting from any ideas, methods, instructions or products referred to in the content.